Elevated A20 promotes TNF-induced and RIPK1-dependent intestinal epithelial cell death

Ricard Garcia-Carbonell[a,b,c,d,1], Jerry Wong[a,b,c,1], Ju Youn Kim[a,b,c], Lisa Abernathy Close[e], Brigid S. Boland[f], Thomas L. Wong[a,b,c], Philip A. Harris[g], Samuel B. Ho[h], Soumita Das[c], Peter B. Ernst[c], Roman Sasik[i,j], William J. Sandborn[f], John Bertin[g], Pete J. Gough[g], John T. Chang[f], Michelle Kelliher[k], David Boone[e], Monica Guma[a,b,c,l,m,2], and Michael Karin[a,b,c,2]

[a]Laboratory of Gene Regulation and Signal Transduction, University of California, San Diego, CA 92093; [b]Department of Pharmacology, University of California, San Diego, CA 92093; [c]Department of Pathology, University of California, San Diego, CA 92093; [d]Department of Biochemistry and Molecular Biology, Faculty of Pharmacy, University of Barcelona, Barcelona, Spain; [e]Department of Microbiology and Immunology, Indiana University School of Medicine, South Bend, IN 46617; [f]Department of Medicine, Division of Gastroenterology, University of California, San Diego, CA 92093; [g]Pattern Recognition Receptor Discovery Performance Unit, Immuno-Inflammation Therapeutic Area, GlaxoSmithKline, Collegeville, PA 19426; [h]Department of Medicine, VA San Diego Healthcare System, San Diego, CA 92161; [i]Center for Computational Biology, University of California, San Diego, CA 92093; [j]Institute for Genomic Medicine, University of California, San Diego, CA 92093; [k]Department of Molecular, Cell and Cancer Biology, University of Massachusetts Medical School, Worcester, MA 01605; [l]Department of Medicine, Division of Rheumatology, University of California, San Diego, CA 92093; and [m]Department of Medicine, Autonomous University of Barcelona, 08193 Bellaterra, Barcelona, Spain

Contributed by Michael Karin, August 14, 2018 (sent for review June 20, 2018; reviewed by Anning Lin and Zheng-Gang Liu)

Intestinal epithelial cell (IEC) death is a common feature of inflammatory bowel disease (IBD) that triggers inflammation by compromising barrier integrity. In many patients with IBD, epithelial damage and inflammation are TNF-dependent. Elevated TNF production in IBD is accompanied by increased expression of the *TNFAIP3* gene, which encodes A20, a negative feedback regulator of NF-κB. A20 in intestinal epithelium from patients with IBD coincided with the presence of cleaved caspase-3, and A20 transgenic (Tg) mice, in which A20 is expressed from an IEC-specific promoter, were highly susceptible to TNF-induced IEC death, intestinal damage, and shock. A20-expressing intestinal organoids were also susceptible to TNF-induced death, demonstrating that enhanced TNF-induced apoptosis was a cell-autonomous property of A20. This effect was dependent on Receptor Interacting Protein Kinase 1 (RIPK1) activity, and A20 was found to associate with the Ripoptosome complex, potentiating its ability to activate caspase-8. A20-potentiated RIPK1-dependent apoptosis did not require the A20 deubiquitinase (DUB) domain and zinc finger 4 (ZnF4), which mediate NF-κB inhibition in fibroblasts, but was strictly dependent on ZnF7 and A20 dimerization. We suggest that A20 dimers bind linear ubiquitin to stabilize the Ripoptosome and potentiate its apoptosis-inducing activity.

apoptosis | inflammatory bowel disease | intestinal epithelial cells | A20 | RIPK1

Crohn's disease (CD) and ulcerative colitis (UC) are common IBDs characterized by intestinal epithelial injury, including mucosal erosion, ulceration, cryptitis, and crypt abscess formation (1). In many patients with IBD, epithelial damage and inflammation depend on TNF, and in most such patients, anti-TNF drugs prevent intestinal epithelial cell (IEC) death and promote healing and mucosal regeneration, at least temporarily (2). Normally, IECs resist TNF-induced death due to activation of NF-κB (3–5), which, in addition to anti-apoptotic genes (6), controls transcription of genes that maintain barrier integrity and microbial homeostasis (7). Hence, the mechanisms that convert TNF to a potent inducer of IEC death and tissue injury in a large fraction of patients with IBD are of importance but remain obscure. Looking for genes that are coregulated with *TNF*, we found a strong correlation between *TNF* and *TNFAIP3* mRNA expression in several different IBD patient cohorts. *TNFAIP3*, which codes for the putative antiinflammatory protein A20, contains three intronic single-nucleotide polymorphisms (SNPs) associated with responsiveness to anti-TNF drugs, such that lower A20 expression correlates with improved drug response (8). Curiously, however, mice with enterocyte-specific A20 deletion are hypersensitive to dextran sodium sulfate (DSS)-induced colitis and TNF-induced epithelial apoptosis (9), effects that are inconsistent with the known ability of A20 to suppress activation of NF-κB (10), which promotes IEC survival (7). Another puzzling finding is induction of early-onset colitis by transgenic (Tg) A20 in IL-10–deficient mice (11). The same A20 Tg mice, however, are protected from DSS-induced, but not 2,4,6-trinitrobenzenesulfonic acid-induced, colitis (12).

A20 contains an N-terminal ovarian tumor (OTU) deubiquitinase (DUB) domain and seven C-terminal ZnF motifs that have been assigned distinct functions, including Lys63 (K63)-linked polyubiquitin binding by ZnF4 and Met1(M1)-linked linear ubiquitin binding by ZnF7 (13). ZnF1 was reported to bind the protein kinase RIPK1, whereas ZnF4 harbors E3 ubiquitin ligase activity (14). Upon TNF receptor 1 (TNFR1) engagement, TNFR1 itself and RIPK1 are modified by the linear and K63-linked ubiquitin ligases cIAP1 and cIAP2, which facilitate

Significance

Excessive apoptosis is detected in the intestinal epithelium of patients with inflammatory bowel disease (IBD), where it is frequently TNF-dependent. We show that A20, a protein implicated in negative regulation of NF-κB, is expressed in intestinal epithelial cells (IECs) from patients with IBD in areas that exhibit apoptosis. Transgenic mice that overexpress A20 in IECs are highly susceptible to TNF-induced cell death. In these mice, A20 potentiates TNF-induced mucosal erosion and RIPK1-dependent IEC apoptosis through Ripoptosome/RIPK1 activation. A20-enhanced IEC damage and intestinal inflammation can be prevented by RIPK1 inhibitors, suggesting a new approach to IBD treatment.

Author contributions: R.G.-C., J.W., M.G., and M. Karin designed research; R.G.-C., J.W., J.Y.K., L.A.C., T.L.W., and M.G. performed research; B.S.B., P.A.H., S.B.H., S.D., P.B.E., R.S., W.J.S., J.B., P.J.G., J.T.C., M. Kelliher, and D.B. contributed new reagents/analytic tools; R.G.-C., J.W., M.G., and M. Karin analyzed data; and J.W., M.G., and M. Karin wrote the paper.

Reviewers: A.L., The University of Chicago; and Z.-G.L., National Cancer Institute.

Conflict of interest statement: P.A.H., J.B., and P.J.G. are employees and shareholders of GlaxoSmithKline. The remaining authors declare no competing financial interests.

[1]R.G.-C. and J.W. contributed equally to this work.

[2]To whom correspondence may be addressed. Email: mguma@ucsd.edu or karinoffice@ucsd.edu.

This article contains supporting information online at www.pnas.org/lookup/suppl/doi:10.1073/pnas.1810584115/-/DCSupplemental.

Published online September 12, 2018.

RIPK1 recruitment to TNFR1 and generate a signaling complex that promotes IκB kinase (IKK)-mediated NF-κB activation (15). By removing K63-linked polyubiquitin, the A20 DUB domain was proposed to prevent RIPK1 interaction with the IKK regulatory subunit IKKγ/NEMO, and by adding K48-linked polyubiquitin, in a ZnF4-dependent manner, A20 was suggested to induce RIPK1 degradation (14). However, mice expressing a ZnF4-deficient A20 variant do not exhibit the same phenotype as *Tnfaip3*-null mice (13, 16), questioning the importance of the E3 ligase activity embedded within ZnF4. Furthermore, a DUB-defective *Tnfaip3* allele does not cause multiorgan inflammation, and fibroblasts homozygous for the DUB deficiency do not show marked differences in TNF-induced NF-κB activation (13, 16, 17). Obviously, not all A20 activities are NF-κB–directed, and its likely involvement and mode of action in IBD pathogenesis merit further investigation.

Results

A20 and Caspase-3 Activation in Human IBD. We examined A20 expression in IBD specimens by comparing ileal and colonic CD transcriptomes with those of healthy tissue. The results revealed strong up-regulation of *TNF* mRNA and other NF-κB target genes, including *TNFAIP3* (Fig. 1*A* and *SI Appendix*, Fig. S1*A*), which was also up-regulated in UC (*SI Appendix*, Fig. S1*A*). Mining of publicly available IBD datasets revealed a strong positive correlation between *TNFAIP3*, *TNF*, and *BIRC3* transcripts (*SI Appendix*, Fig. S1*B*), suggesting that A20 may not inhibit NF-κB–mediated transcription in IBD tissues. Furthermore, most patients with high *TNF* mRNA also showed high *TNFAIP3* mRNA (*SI Appendix*, Fig. S1*C*). Immunohistochemical (IHC) analysis revealed that A20 was up-regulated in both lamina propria cells and IECs of active IBD tissue and that its expression in IECs correlated with that of cleaved caspase-3 (cC-3; $P < 0.0001$, $r = 0.73$; $n = 23$ samples), which marks apoptotic cells (Fig. 1*B* and *SI Appendix*, Fig. S2 and Table S1). The level of inflammation reported for these samples showed a modest correlation with A20 ($P < 0.0085$, $r = 0.49$; $n = 23$ samples) and cC-3 ($P = 0.05$, $r = 0.4$; $n = 23$ samples) expression (*SI Appendix*, Fig. S3), further confirming A20 up-regulation and apoptosis in inflamed IBD tissues.

TNF-Induced Apoptosis in A20 Tg Mice. A20 expression in IECs was reported to either restrain apoptosis and maintain barrier function (9, 18) or promote development of colitis (11), two diametrically opposed outcomes, neither of which is fully consistent with A20-mediated inhibition of NF-κB signaling. To determine how elevated A20 affects the viability of TNF-exposed IECs, we used villin-*Tnfaip3* (hereafter A20) Tg mice (18). These mice are healthy and display normal growth and intestinal development (12), but after i.v. injection of 1 μg of murine TNF, all A20 Tg mice died within 6 h, whereas all C57BL/6 (hereafter B6) control mice survived (*SI Appendix*, Fig. S4 *A* and *B*). TNF-challenged A20 Tg mice exhibited a markedly elevated septic score and a dramatic drop in body temperature (*SI Appendix*, Fig. S4*B*). TNF-challenged A20 Tg mice showed enhanced IL-6 production with a mild increase in lung inflammatory infiltrates and splenic architecture disruption but no obvious damage to the kidneys or liver (*SI Appendix*, Fig. S4 *D* and *E*). TNF challenge resulted in extensive mucosal erosion, with complete loss of villi in the small bowel, and caspase-3 activation in the small intestine and large intestine of A20 Tg mice (Fig. 1 *C* and *D*).

TNF-Induced Apoptosis in A20-Expressing Enteroids. A20 Tg mice that are IL-10–deficient exhibit defective expression of mucosal cytokines and antimicrobial peptides, resulting in microbial colonization of the inner mucus layer, along with microbial dysbiosis (11). To assess IEC-autonomous A20 effects, we used enteroid (intestinal organoid) cultures, which retain normal epithelial differentiation and are free of microbes and immune cells (19). Whereas B6 enteroids remained intact, A20 Tg enteroids underwent extensive TNF-induced cell death, especially within villus domains (Fig. 2 *A* and *B*). Four hours after TNF challenge, immunofluorescence analysis revealed cC-3 in A20 Tg enteroid villus domains (Fig. 2*B*), consistent with TNF-induced villus erosion in vivo (Fig. 1*D*). A20 Tg enteroids also showed strong cC-3/cC-8 expression by immunoblotting (IB), whereas control enteroids were unaffected (Fig. 2*C*), indicating that immune cells and gut microbiota are not needed for TNF-induced apoptosis of A20-expressing IECs. We validated these findings by transducing control enteroids with a doxycycline (DOX)-inducible A20 (iA20) construct. A20 induction strongly potentiated TNF-induced caspase activation (Fig. 2*D*), indicating that the results are not due to any reprogramming that is peculiar to A20 Tg mice.

A20 Has a Minor Effect on NF-κB Activation and Transcriptional Activity in IECs. As found in human IBD specimens, elevated A20 did not reduce mRNA and protein expression of anti-apoptotic genes and NF-κB–related molecules in the small intestine and large intestine of A20 Tg mice (Fig. 3 *A* and *B*). A20 Tg and DOX-treated iA20 enteroids also did not show any defect in expression of antiapoptotic genes and NF-κB–related molecules (Fig. 3*C*). TNF-induced IκBα degradation was slightly decreased in A20-expressing enteroids (Fig. 3*D*). Likewise, IKK activation was partially blunted in A20 Tg organoids (Fig. 3*E*), but iA20 expression had a miniscule effect on IKK activation (Fig. 3*F* and *SI Appendix*, Fig. S8 *B* and *C*), although it fully potentiated TNF-induced cell death (Fig. 2*D*). Moreover, although expression of some NF-κB target genes was reduced at baseline in A20 Tg enteroids, their TNF-induced expression was marginally affected by DOX-induced iA20 (*SI Appendix*, Fig. S5 *A* and *B*). These results are generally consistent with lower A20 levels in iA20 enteroids relative to Tg A20 (Fig. 3*C*) and suggest that TNF-induced apoptosis in A20-expressing cells was not secondary to NF-κB inhibition and decreased antiapoptotic gene expression. Thus, unlike its effect in other cell types (20), A20 has only a minor effect on NF-κB signaling in IECs.

RIPK1 Activity Is Required for A20-Potentiated TNF-Induced Apoptosis. TNF-induced cell death depends on formation of death-inducing signaling complexes. Whereas complex IIa mediates classical apoptosis when synthesis of antiapoptotic proteins is inhibited, complex IIb, also known as the Ripoptosome because of its dependence on RIPK1 activity, mediates apoptosis in cells treated with second mitochondria-derived activator of caspase (SMAC) mimetics that induce cIAP1/2 degradation (15). By contrast, complex III, whose activity depends on both RIPK1 and RIPK3, mediates programmed necrosis when caspase activity is blocked (21). We used pharmacological inhibitors of RIPK1 [Necrostain-1 (Nec-1), Nec-1s, and GSK′963] and RIPK3 (GSK′843 and GSK′872) (22–24) to discern the involvement of RIPK1 and RIPK3 in TNF-induced death of A20-expressing IECs. Whereas RIPK1 inhibitors prevented TNF-induced cell death and caspase activation, RIPK3 inhibitors did not (Fig. 4 *A* and *B*). Similar results were obtained in iA20 enteroids (Fig. 4*C*). However, iA20 expression in enteroids derived from *Ripk1* kinase dead knock-in mice ($Ripk1^{KDKI}$) (25) did not sensitize the cells to TNF-induced apoptosis (Fig. 4*D*). Furthermore, administration of the RIPK1 inhibitor GSK′963 by i.p. injection to A20 Tg mice 1 h before TNF challenge greatly improved the septic score and inhibited mucosal erosion (Fig. 4 *E* and *F*). Of note, the RIPK1 inhibitor did not block cytokine and inflammatory gene induction on TNF challenge (*SI Appendix*, Fig. S6).

A Critical Role for ZnF7 in TNF-Induced RIPK1-Dependent IEC Death. RIPK1 activation and its proapoptotic activity are triggered upon

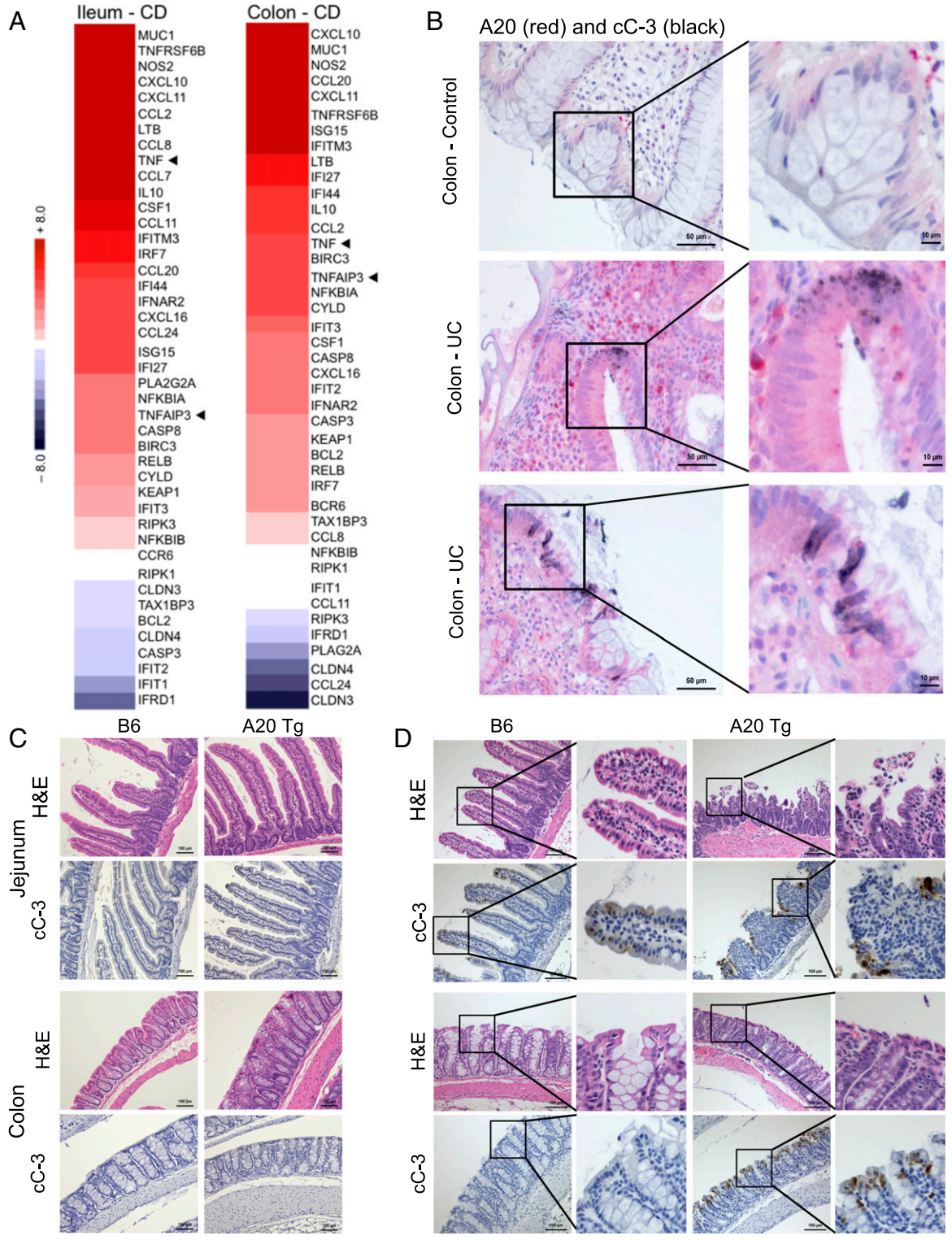

Fig. 1. Increased TNFAIP3 (A20) expression in human IBD specimens and mice correlates with IEC apoptosis. (*A*) Heat maps of IBD-related genes that are differentially expressed between ileal ($n = 3$) and colonic ($n = 3$) CD and healthy tissue. (*B*) IHC double staining of cC-3 (black) and A20 (red) in control and UC colonic sections. (Scale bars: *Left*, 50 μm; *Right*, 10 μm.) Representative H&E and cC-3 IHC staining of jejunal and colonic sections from B6 and A20 Tg mice at time 0 (*C*) and 4 h after TNF injection (*D*) is shown (1 μg administered i.v., $n = 5$). (Scale bars: 100 μm.)

its incorporation into the Ripoptosome, which also contains C8, cFLIP, and FADD (15, 26–28). FADD immune complexes from TNF (T)-stimulated A20-expressing enteroids that were briefly treated with Z-VAD-FMK (Z) to retain active C8 within the Ripoptosome (15) contained much more cC-8 than FADD complexes from T + Z-incubated B6 enteroids (Fig. 5*A*). Importantly, A20 was also present in FADD immune complexes from T + Z-stimulated A20-expressing enteroids (Fig. 5*A*),

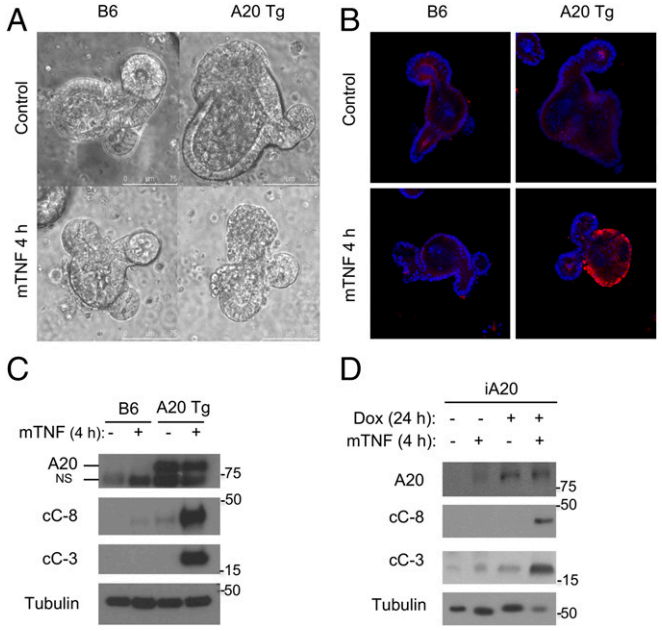

Fig. 2. Elevated A20 sensitizes enteroids to TNF-induced apoptosis. (*A*) Bright-field images of B6 and A20 Tg enteroids at time 0 and 4 h after TNF (40 ng/mL) addition. (Magnification: 200×.) (*B*) Confocal images of cC-3–stained enteroids after TNF addition as in *A*. (Scale bars: 50 μm.) (*C*) IB of B6 and A20 Tg enteroids with or without TNF (40 ng/mL) stimulation. (*D*) IB of iA20 enteroids incubated with or without DOX (1 μg/mL for 24 h) before TNF addition. mTNF, mouse TNF; NS, nonspecific band.

suggesting that A20 enhances Ripoptosome formation by interacting with one of its components. Of note, B6 enteroids treated with cycloheximide (CHX) and incubated with T + Z, a combination that triggers TNF-induced cell death independent of RIPK1 activation (*SI Appendix*, Fig. S7*A*), exhibit minimal C8 or A20 recruitment to FADD (Fig. 5*A*). As expected, addition of Nec-1 to inhibit RIPK1 prevented the appearance of cC-8 in the FADD immune complexes. Expression of cIAP1, whose degradation promotes Ripoptosome formation (15), was similar in B6- and A20-expressing IECs and enteroids (Fig. 3 *B* and *C*), indicating that A20 does not operate by suppressing cIAP1 expression.

RIPK1 is modified by K63-linked polyubiquitin (13), whose removal by CYLD facilitates Ripoptosome formation (15). As A20 can also remove K63-linked polyubiquitin from RIPK1 (14), we examined the ubiquitination status of TNFR1-associated RIPK1, expecting to find less ubiquitinated RIPK1 in A20 Tg enteroids. Much to our surprise, A20 expression attenuated the deubiquitination of TNFR1-bound RIPK1, which was almost complete in B6 enteroids at 60 min after TNF addition (Fig. 5*B*). Furthermore, A20 expression increased the amount of TNFR1-bound RIPK1. In contrast, CHX pretreatment had no effect on deubiquitination of TNFR1-bound RIPK1 (*SI Appendix*, Fig. S7*B*), further demonstrating that the mechanism that promotes TNF-induced cell death after NF-κB inhibition (by CHX) is distinct from the one that accounts for A20-enhanced Ripoptosome formation. As reported (13), A20 itself was incorporated into the TNFR1 signaling complex (Fig. 5*B*). Of note, CYLD protein expression was similar in B6- and A20-expressing IECs and enteroids (Fig. 3*C*).

We conducted mutational analysis to identify A20 functional domains required for enhancement of TNF-mediated caspase activation. Inducible A20 variants lacking either DUB activity due to a C103A OTU domain substitution (14) or K48-linked E3 ligase function (C609A/C612A), which resides in ZnF4 (13), were as effective as WT iA20 in sensitizing IECs to TNF-induced apoptosis (*SI Appendix*, Fig. S8*A*). Next, we examined the role of ZnF7, which is required for binding of linear polyubiquitin (29), using a C764A/C767A double-substitution mutant. Notably, expression of the ZnF7 mutant failed to enhance TNF-induced caspase activation, whereas the OTU-deficient mutant was fully functional (Fig. 5*C*). Of note, the different A20 mutations had minor effects on inhibition of IKK activation, which was barely noted even for WT iA20 (*SI Appendix*, Fig. S8). Most importantly, the ZnF7 mutant was not recruited to FADD and was compromised in enhancement of Ripoptosome formation/C8 activation (Fig. 5*D*).

A Critical Role for A20 Homodimerization in TNF-Induced RIPK1-Dependent IEC Death. A20 forms homodimers through a dimerization surface within its N-terminal portion (16). We generated a homodimerization-restricted (HR) iA20 variant containing M15A, R16E, and H351A substitutions (16). The iA20HR variant failed to potentiate TNF-induced cell death (Fig. 6*A*), although it was efficiently expressed and as capable of modest IKK/NF-κB inhibition as WT A20 (Fig. 6 *B* and *C*). Of note, iA20HR was compromised in its association with FADD complexes and failed to potentiate C8 activation/Ripoptosome formation (Fig. 6*D* and *SI Appendix*, Fig. S9). Collectively, these results suggest that A20 facilitates Ripoptosome assembly by binding as a dimer to linear ubiquitin chains via ZnF7, thereby protecting RIPK1 from deubiquitination, stabilizing the Ripoptosome complex, and enhancing caspase-8 recruitment and activation (Fig. 7).

Discussion

Genome-wide association studies identified *TNFAIP3* as a disease susceptibility locus in several inflammatory diseases, including IBD (29). However, most disease-associated SNPs within the *TNFAIP3* locus are located in noncoding regions, and their effects on A20 expression and IBD pathogenesis are unknown (29). Furthermore, SNPs that reduce A20 expression are associated with improved response to anti-TNF drugs (8). Nonetheless, it is unknown within what types of cells A20 acts to influence IBD pathogenesis. We found that A20 is highly expressed in the mucosa of patients with IBD and that its elevated expression in IECs is associated with caspase-3 activation, likely causing barrier deterioration and intestinal inflammation. Using Tg mice expressing A20 in IECs (18), we found that elevated A20 greatly enhances susceptibility to TNF-induced apoptosis, resulting in barrier deterioration and acute inflammation. These findings challenge the view that A20 is predominantly an antiinflammatory protein, which is based on the ability of A20 ablation to cause severe inflammation through TNF-dependent and -independent pathways (13, 14, 30). Of all different forms of TNF-induced cell death, A20 specifically potentiates RIPK1-dependent apoptosis (also known as ripoptosis), a phenomenon originally identified in cultured cells treated with SMAC mimetics (15), but heretofore not shown to occur in vivo. In some cells, A20 functions as a feedback inhibitor of NF-κB (10, 20), an activity that depends on removal of K63-linked polyubiquitin chains from RIPK1 via A20 DUB activity and addition of K48-linked polyubiquitin via A20 ZnF4 (13, 14). However, in vivo studies have failed to reveal a major effect of A20 on NF-κB (16, 17), although inactivation of its OTU/DUB domain or ZnF4 enhanced both p38 and JNK activation (13). Furthermore, in IECs, A20 had little effect on NF-κB signaling and actually slowed down deubiquitination of TNFR1-bound RIPK1. In addition, recent work showed that A20's functions depend on interactions with other proteins (13, 31, 32). It is therefore plausible that the availability of these secondary mediators as well as the stoichiometry of complexes that form downstream of the TNF receptor may vary depending on the cell type, which would explain an enhanced cell death instead of

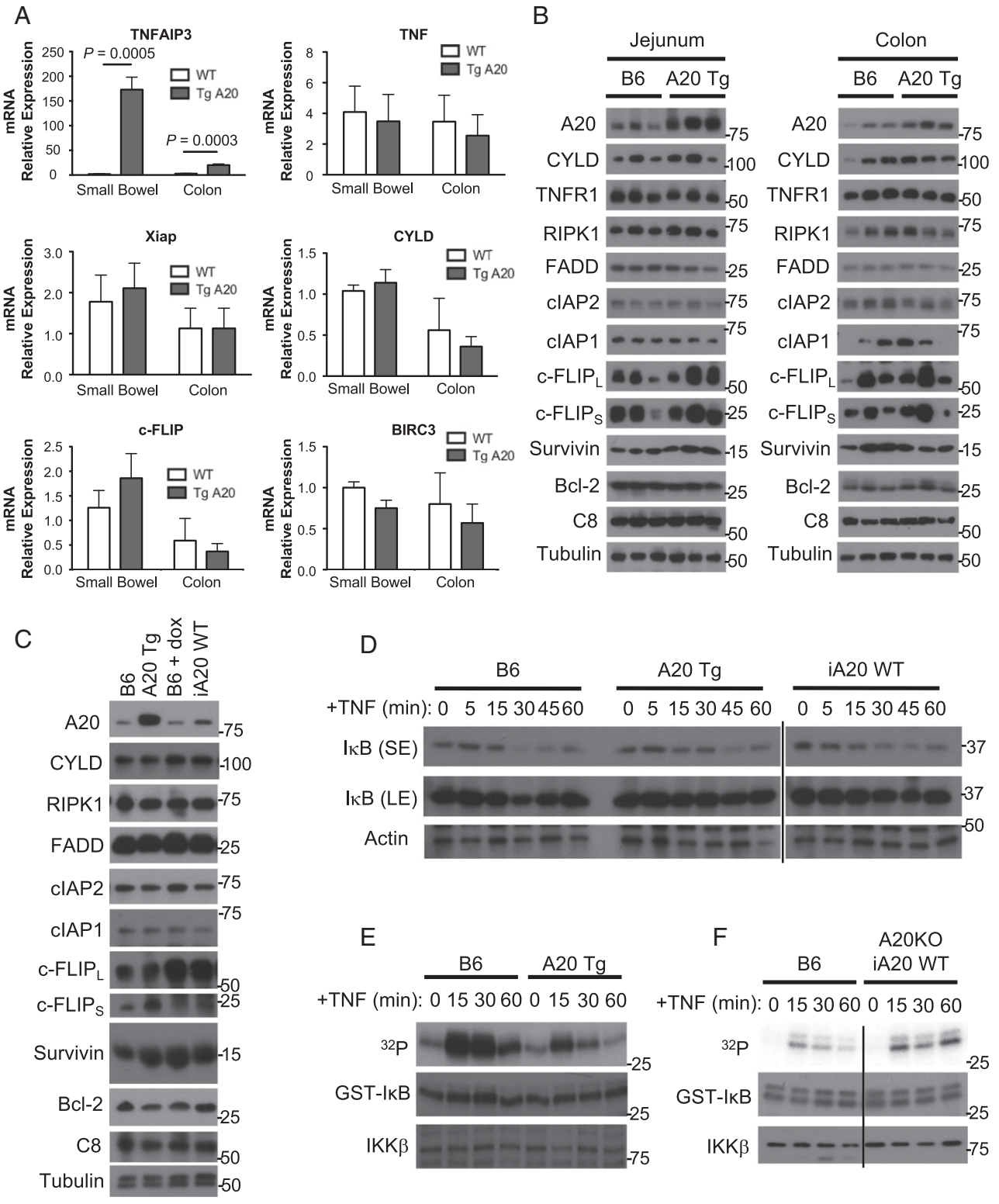

Fig. 3. Elevated A20 has a minimal effect on NF-κB signaling in IECs and enteroids. (*A*) Real-time qPCR analysis of the indicated transcripts in jejunal and colonic IECs from B6 and A20 Tg mice. Results are mean ± SEM. (*B*) IB analysis of jejunal and colonic lysates from B6 and A20 Tg mice. (*C*) IB analysis of lysates of untreated and DOX-treated B6, A20Tg, and iA20-transduced enteroids. (*D*) IB analysis of indicated proteins in lysates of B6, A20Tg, and DOX-treated iA20 enteroids stimulated with TNF. (*E* and *F*) IKK activity was assessed by immune complex kinase assay using GST-IκBα(1–54) as a substrate in lysates of the indicated enteroids (the images in *F* are taken from the blot shown in *SI Appendix*, Fig. S8*B*).

complete NF-κB pathway blockade. Indeed, A20 itself is recruited into the Ripoptosome complex in a manner dependent on its ZnF7, which exhibits high affinity to linear ubiquitin chains (13). Neither the OTU/DUB domain nor ZnF4 is involved in Ripoptosome recruitment and activation. Given the dependence of Ripoptosome recruitment on ZnF7, it is plausible that

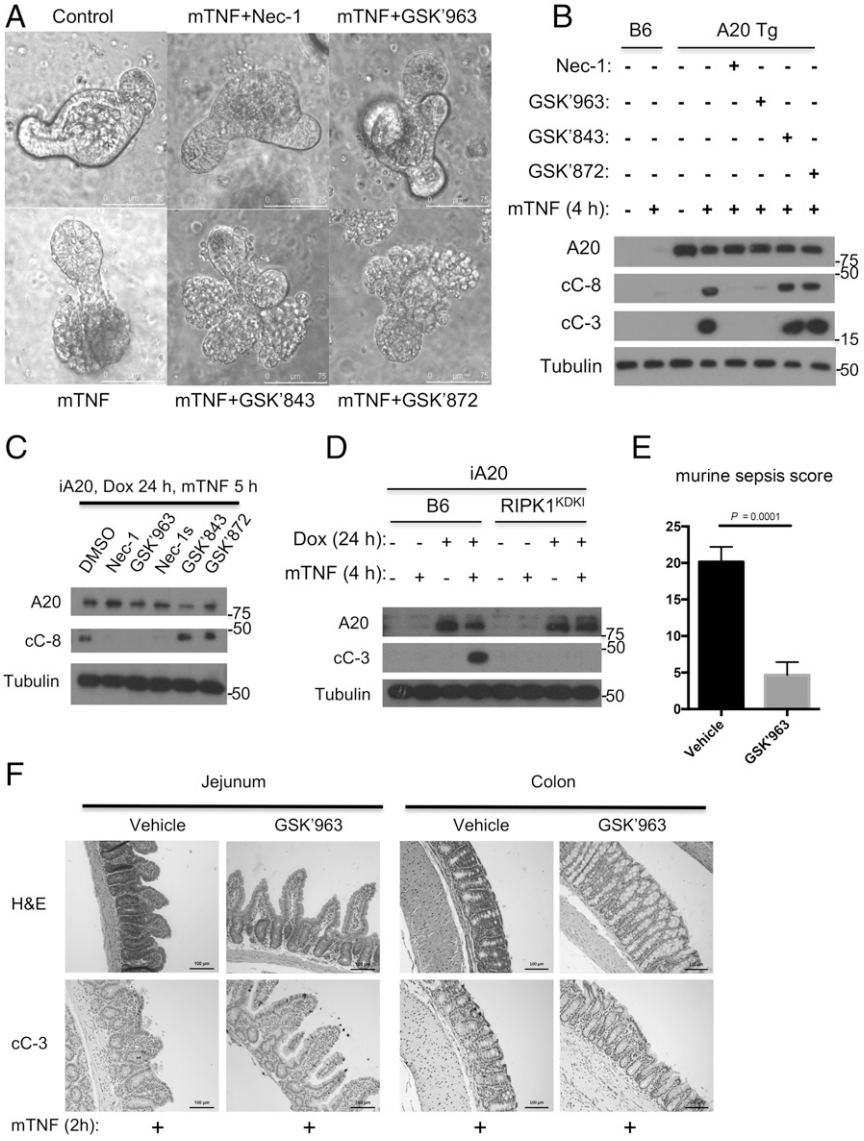

Fig. 4. TNF-induced apoptosis of A20-expressing IECs depends on RIPK1 kinase activity. (*A*) Bright-field images of A20 Tg enteroids incubated with TNF for 4 h without or with RIPK1 or RIPK3 inhibitors. mTNF, mouse TNF. (Magnification: 200×.) (*B*) IB analysis of B6 and A20 Tg enteroids treated as above. (*C*) IB analysis of iA20-transduced B6 enteroids after 24-h DOX pretreatment and TNF stimulation for 5 h without or with RIPK1 or RIPK3 inhibitors. (*D*) IB analysis of iA20-transduced B6 or *Ripk1*^{KDKI} enteroids after DOX pretreatment and TNF stimulation. (*E*) Murine sepsis scores of five A20 Tg mice after TNF (1 μg) injection without or with GSK′963 (50 mg/kg). Results are mean ± SD. $P < 0.0001$. (*F*) H&E or cC-3 staining of jejunal and colonic sections from A20 Tg mice injected with TNF in the absence or presence of GSK′963. (Scale bars: 100 μm.)

A20 may bind to the linear ubiquitin chains attached to K115 of RIPK1 (33–35). By binding linear ubiquitin chains, A20 can inhibit their degradation or removal (36, 37). Notably, inactivation of HOIP, the ubiquitin ligase subunit of the linear ubiquitination assembly complex (LUBAC), prevents A20 recruitment to the TNFR1 signaling complex (36), a finding consistent with our suggestion that A20 binds RIPK1 once the latter has been subject to LUBAC-mediated linear ubiquitination.

A20-enhanced, TNF-induced Ripoptosome formation is prevented by ZnF7 inactivation or restriction of A20 homodimerization. These findings suggest that A20 binds to RIPK1 linear ubiquitin chains as a dimer, thereby stabilizing the Ripoptosome and potentiating activation of its caspase-8 moiety via induced proximity (Fig. 7). A similar model was proposed to explain TRAIL-induced caspase-8 activation. Although, by themselves, caspase-8 dimers are unstable and may fall apart once released from the death-inducing signaling complex (DISC) (38, 39), the binding of p62/SQSTM1 to caspase-8–linked K63 polyubiquitin chains enhanced caspase-8 oligomerization and activation (40).

Much of the biochemical information gathered about A20 and its participation in TNF signaling was obtained using fibroblasts, in which A20 restricts NF-κB signaling. Although A20 weakly attenuates NF-κB activation in IECs, it does not inhibit expression of NF-κB–dependent antiapoptotic genes. Furthermore, while NF-κB inhibition was reported to depend on the A20 DUB and ZnF4 motifs (13), neither of these motifs affects RIPK1 activation and TNF-induced cell death. Thus, the ability of A20 to enhance TNF-induced apoptosis is not due to NF-κB inhibition, which facilitates complex IIA-dependent apoptosis (21). We propose that elevated A20 expression is an important contributor to barrier disruption and initiation of microbiota-dependent inflammation in patients with IBD who produce higher than normal amounts of TNF. Of note, the complete absence of A20 is not healthy either, as it also increases the

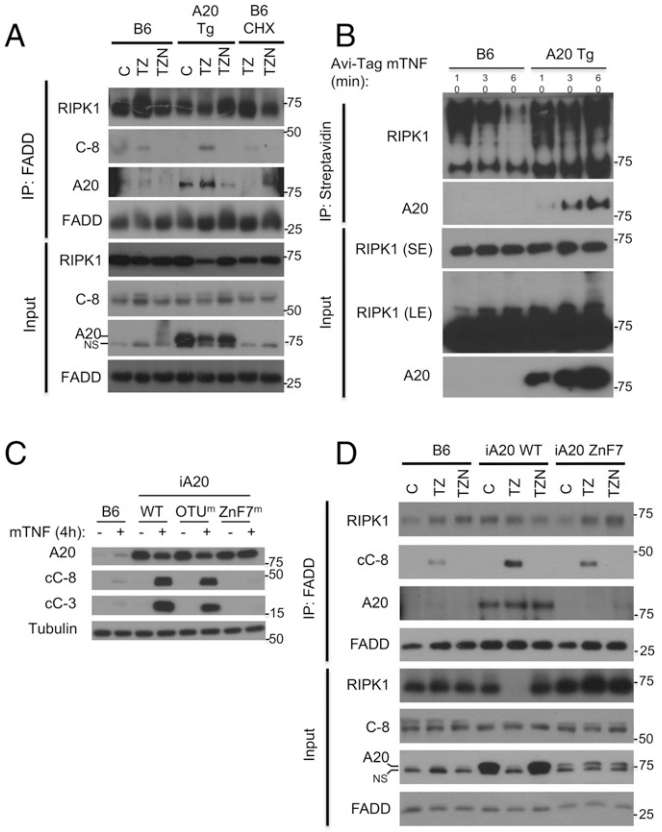

Fig. 5. A20 enhances Ripoptosome activation and slows down deubiquitination of TNFR1-bound RIPK1. (*A*) FADD immunoprecipitates from B6 and A20 Tg enteroids stimulated without (C) or with TNF (20 ng/mL) + zVAD (10 μg/mL) (TZ) or TZ + Nec1 (50 μM) (TZN) in the absence or presence of cycloheximide (CHX) were analyzed by IB as indicated. (*B*) TNFR1 immunoprecipitates from B6 and A20 Tg enteroids stimulated with AviTag mTNF (10 ng/mL) were analyzed by IB as indicated. (*C*) Lysates of B6 enteroids transduced with the indicated iA20 constructs and treated with DOX and/or TNF were analyzed by IB as indicated. (*D*) FADD immunoprecipitates of B6-deficient or A20-deficient enteroids transduced with the indicated iA20 constructs and pretreated with DOX (as in *C*) before addition of TZ or TZN as indicated. NS, nonspecific band.

susceptibility to TNF-induced IEC death and microbial translocation (9). This effect, however, is dependent on necroptosis and can be blocked by RIPK3 ablation (41). The TNF-induced death of A20-expressing IECs, however, can only be prevented by RIPK1 inhibitors.

Experimental Procedures

Mice. A20-Tg mice have been described (18). *A20-Tg;Rag1*$^{+/-}$ mice were used for the in vivo experiments described herein. *Ripk1*^{D138N} mice were obtained from Vishva Dixit (Genentech) (42). Experimental animals were 8–12 wk of age, all in the B6 genetic background, and maintained under specific-pathogen-free (SPF) conditions at a University of California, San Diego (UCSD) animal facility accredited by the American Association for Accreditation of Laboratory Animal Care. All studies were conducted in accordance with the GSK Policy on the Care, Welfare, and Treatment of Laboratory Animals, and all animal protocols were approved by the UCSD Institutional Review Board (IRB) following NIH guidelines. Mice were fed autoclaved standard chow, and all of the different strains were cohoused to minimize microbiome fluctuations.

Reagents. TNF (R&D Systems) was injected at 2 μg per mouse unless otherwise indicated. In vitro, TNF was used at 40 ng/mL. DOX (1 μg/mL), zVAD-FMK (50 μM), and BHA (10 μM) were purchased from Sigma. Necrostatin-1 (100 μM) was purchased from Calbiochem. The RIPK1 (963: 50 nM) and the RIPK3 (843: 5 μM, 872: 5 μM) inhibitors were synthesized at GSK and purified before use (23, 24). For in vivo studies, GSK′963 (50 mg/kg) was dissolved in saline with 5% DMSO and 6% Cavitron, and injected i.p.

Human Samples. Archived colonic specimens for IHC analyses were obtained from patients who underwent routine colonoscopy and were histologically scored by an independent pathologist. Prospective colonic specimens for RNA analysis were obtained from patients with CD and UC and from healthy controls undergoing colonoscopy as part of routine medical care at UCSD. The participants had a diagnosis of CD or UC and were at least 18 y of age. Healthy controls had undergone routine colonoscopy and were not included if they reported gastrointestinal symptoms. Patients' clinical status was verified by chart review of all medical records and laboratory and pathologic data, and all specimens were deidentified before use. All participants provided written informed consent, and studies were approved by the IRB at UCSD and the VA San Diego Healthcare System.

RNA Sequencing and Bioinformatics. Total RNA was isolated from human intestinal tissues and assessed for quality using an Agilent Bioanalyzer, and samples with an RNA integrity number of 7 or greater were used to generate cDNA libraries using Illumina's TruSeq Stranded Total RNA Sample Prep Kit starting with 100 ng of RNA. Libraries were sequenced on an Illumina HiSeq2500 sequencer. Fastq files were aligned to the human transcriptome of the Genome Reference Consortium GRCh.37/hg19, using the STAR aligner (43). Transcript-level counts were calculated with the expectation maximization algorithm RSEM (44). Transcript-level summaries were processed into gene-level summaries by combining all transcript counts from the same gene. Gene counts from different samples were normalized and analyzed for differential expression using DESeq (45). Since at least one of the samples does not have biological replicates, we used an approach in which dispersion of gene counts is estimated from all available samples as if they were replicates. All presented measures of statistical significance should be viewed in this light.

Real-Time qPCR. Total RNA was extracted with TRIzol (Invitrogen) and reverse-transcribed with random hexamers and a SuperScript II Kit (Invitrogen). qPCR was performed with a SYBR Green PCR Master Mix Kit (Applied Biosystems). Relative transcript amounts were compared with those of GAPDH mRNA and

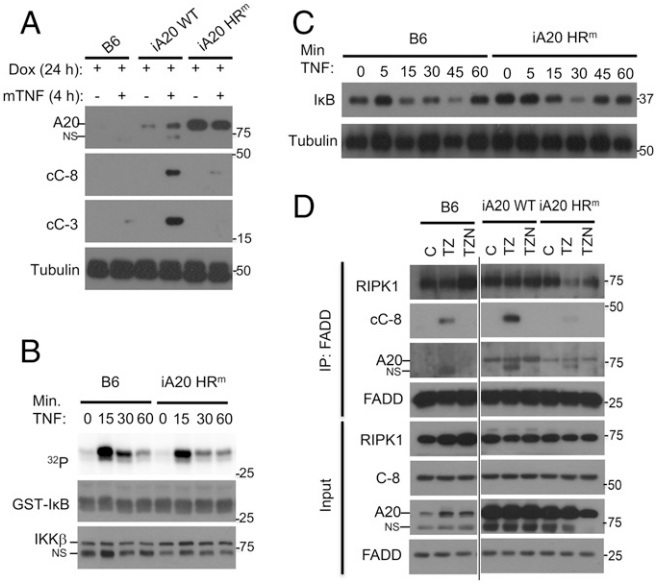

Fig. 6. A20 dimerization is required for enhancement of RIPK1-dependent apoptosis. (*A*) Lysates of B6- or A20-deficient enteroids transduced with the indicated iA20 constructs that were DOX-pretreated and TNF-stimulated were analyzed by IB as indicated. mTNF, mouse TNF. (*B*) IKK activity measured by immune complex kinase assay in lysates of B6- and iA20HR-expressing A20-deficient enteroids before and after TNF addition. (*C*) Lysates of B6- and iA20HR-expressing enteroids treated as above were analyzed by IB for IκBα expression. (*D*) FADD immunoprecipitates of B6- or A20-deficient enteroids transduced with indicated iA20 constructs that were pretreated with DOX (as in *C*) and then stimulated with TZ or TZN were analyzed by IB for the indicated proteins (full figure in *SI Appendix*, Fig. S9). NS, nonspecific band.

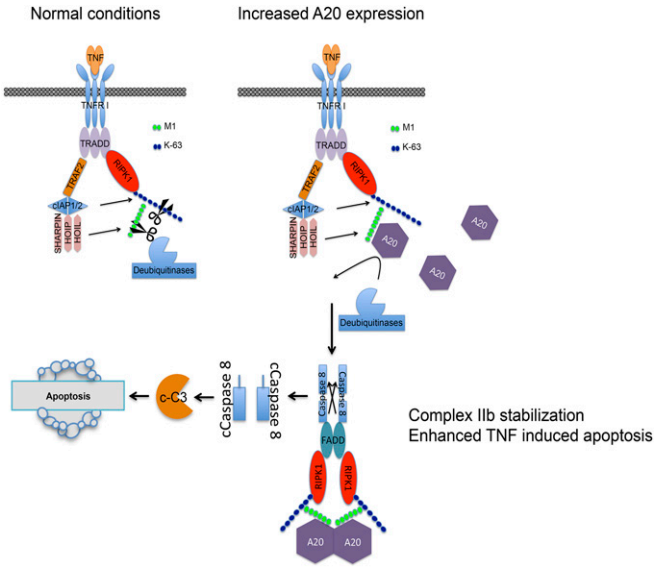

Fig. 7. Model explaining how A20 dimerization and binding to linear ubiquitin via ZnF7 enhances Ripoptosome assembly and RIPK1-dependent apoptosis in TNF-stimulated IECs.

normalized to untreated samples by the delta-delta Ct ($^{\Delta\Delta}$Ct) method. Primers are available upon request.

Histological and Immunohistochemical Analyses. Intestines were removed, opened longitudinally, cleaned, processed as "Swiss rolls," and fixed in 10% phosphate-buffered formalin for 24 h. Formalin-fixed tissues were paraffin-embedded, and 5-μm sections were prepared and stained with H&E. For IHC analysis, mouse and human tissue sections were incubated overnight at 4 °C with cC-3 antibodies (9661; Cell Signaling) at a 1:200 dilution. Antigen retrieval was with citrate buffer (pH 6.0) at 96 °C for 20 min. For double-staining IHC, antigen retrieval was achieved by boiling the samples for 30 min in citrate buffer at pH 6.0. Tissue sections were incubated overnight with an A20 primary antibody (ab111192) in PBS plus 3% BSA, and then incubated with secondary alkaline phosphatase-linked antibody (1:200, AP-9500) at room temperature for 1 h. After washing, slides were developed using VectorRed (SK-5100; Vector Laboratories). Slides were further washed and incubated overnight with the second primary antibody against cC-3 (9661; Cell Signaling). Samples were then incubated with the secondary HRP-conjugated antibody (MP-7401; Vector Laboratories) and developed with diaminobenzidine solution plus nickel (SK-4100; Vector Laboratories). All sections were counterstained with hematoxylin and photographed using an Axioplan 200 microscope with AxioVision Release 4.5 software (Zeiss).

Enteroid Isolation and Culture. Small intestinal organoids (enteroids) were cultured as described (19). Briefly, crypts were collected from mouse small intestine after a 30-min incubation in PBS (pH 7.4) containing 2 mM EDTA at 4 °C. Enteroids were plated in Matrigel (BD Bioscience) and maintained in DMEM/F12 (Life Technologies) containing B27 and N2 supplements (Life Technologies), 1.25 mM *N*-acetyl L-cysteine (Sigma), 100 ng/mL noggin (GoldBio), 50 ng/mL mouse EGF (mEGF) (Biosource), and 10% Rspo1-Fc–conditioned medium (the Rspo1-Fc–expressing cell line was a generous gift from Calvin Kuo, Stanford University, Stanford, CA).

Immunoblotting and Immunoprecipitation. Whole-cell extracts were obtained by lysing enteroids in ice-cold radioimmunoprecipitation assay lysis buffer (Cell Signaling) containing 20 mM Tris·HCl (pH 7.5), 150 mM NaCl, 10 mM EDTA, 1% Triton X-100, and 1% deoxycholate, supplemented with a protease and phosphatase inhibitor mixture (Roche). Proteins were separated by SDS/PAGE and transferred to nitrocellulose membranes that were incubated with antibodies against IκBα (Santa Cruz Biotechnology), RIPK1, CYLD, cC-3, cC-8, A20, cIAP1, caspase-8, FADD (Cell Signaling), actin, and tubulin (Sigma). For immunoprecipitation (IP) experiments, enteroids were incubated with 100 μg/mL AviTag-mouse TNF (mTNF) for 1 h on ice and then at 37 °C for 10, 30, and 60 min before collection. Cell extracts were immunoprecipitated with biotinylated magnetic beads (CST). In other experiments, we used FADD antibody and Protein G Dynabeads (Life Technologies) overnight at 4 °C. Immune complexes were washed with lysis buffer and analyzed by IB. To isolate protein complexes by co-IP, the indicated antibodies and cell lysates were incubated in 10 mM Tris (pH 7.4), 150 mM NaCl, and 0.2% Nonident P-40.

Immunofluorescence. Enteroids in Matrigel were fixed with 4% paraformaldehyde overnight at 4 °C. Fixed enteroids were blocked with PBS containing 0.2% Triton X-100 and 1% BSA for 30 min and then immunostained with primary antibodies overnight at 4 °C and with Alexa Fluor 594-conjugated goat anti-rabbit IgG secondary antibody for 1 h at room temperature. Immunostained enteroids were gently mounted on glass slides and imaged under a Leica confocal microscope.

Constructs and Lentivirus Transduction of Enteroids. Inducible-A20 lentiviral expression constructs were made by subcloning PCR-amplified *att*B-flanked full-length A20 (14) and the different A20 mutants (16). cDNAs were PCR-amplified and cloned into pINDUCER20 (46) using the Gateway Clonase II system (Life Technologies). All constructs were verified by sequencing.

Lentiviral constructs were transfected along with pMD2.G (Plasmid 12259; Addgene) and psPAX2 (Plasmid 12260; Addgene) into 293T cells to produce viral particles used to infect enteroids as described (47). Briefly, 2 d before virus infection, enteroids were supplemented with 50% Wnt3a conditioned medium (the Wnt3a-expressing cell line was a generous gift from Karl Willert, UCSD) and 10 mM nicotinamide. Single cells were obtained by digesting the enteroids with TrypLE (Life Technologies) for 5 min at 37 °C. Cells were mixed with high-titer lentivirus plus polybrene (8 μg/mL; Santa Cruz Biotechnology) and Y-27632 (10 μM; Sigma) in a 48-well culture plate and centrifuged at 600 × *g* at 32 °C for 60 min, followed by a 5-h incubation at 37 °C. Cells were then plated in Matrigel and cultured in media with 50% Wnt3a, nicotinamide, and Y-27632 for 2 d, followed by selection with puromycin (1 μg/mL) or G418 (800 ng/mL) in regular media for 1 wk.

Statistical Analysis. Statistical analysis was performed with Prism software (version 5; GraphPad). Results are expressed as mean ± SEM if not otherwise indicated. Normality of the variables was assessed using the Kolmogorov–Smirnov and D'Agostino–Pearson normality tests. For comparison between two groups, the Student's two-tailed *t* test or nonparametric Mann–Whitney test was applied, depending on the normality of the distribution of the variables. We compared three or more groups with analysis of variance; either Dunnett's post hoc test or the Bonferroni test was chosen, depending on the homogeneity of variances. For correlation studies, the Pearson or Spearman test was applied depending on the normality of distribution of the variables. Results were considered significant if the two-sided *P* value was less than 0.05.

ACKNOWLEDGMENTS. We thank Genentech and Dr. Vishva Dixit for the provision of *Ripk1*^{D138} mice. J.W. and R.G.-C. were supported by fellowships from the Canadian Institutes of Health Research and Boehringer Ingelheim Fonds, respectively. M.G. and B.S.B. were supported by NIH Grants K08AR064834 and KL2TR001444, respectively. P.B.E. was supported by the Wayne and Gladys Valley Foundation and the NIH (Grant AI079145). This study was also supported by NIH Grant R01DK093507 (to J.T.C.) and UCSD Digestive Disease Research Development Center Grant DK080506. M. Karin was supported by grants from the NIH (Grant R01AI043477) and Alliance for Lupus Research (Grant 257214), is an American Cancer Society Research Professor, and holds the Ben and Wanda Hildyard Chair for Mitochondrial and Metabolic Diseases.

1. Abraham C, Cho JH (2009) Inflammatory bowel disease. *N Engl J Med* 361:2066–2078.
2. Zeissig S, et al. (2004) Downregulation of epithelial apoptosis and barrier repair in active Crohn's disease by tumour necrosis factor alpha antibody treatment. *Gut* 53:1295–1302.
3. Chen CD, et al. (2004) Molecular determinants of resistance to antiandrogen therapy. *Nat Med* 10:33–39.
4. Greten FR, et al. (2004) IKKbeta links inflammation and tumorigenesis in a mouse model of colitis-associated cancer. *Cell* 118:285–296.
5. Nenci A, et al. (2007) Epithelial NEMO links innate immunity to chronic intestinal inflammation. *Nature* 446:557–561.
6. Lin A, Karin M (2003) NF-kappaB in cancer: A marked target. *Semin Cancer Biol* 13:107–114.
7. Pasparakis M (2009) Regulation of tissue homeostasis by NF-kappaB signalling: Implications for inflammatory diseases. *Nat Rev Immunol* 9:778–788.
8. Vereecke L, et al. (2014) A20 controls intestinal homeostasis through cell-specific activities. *Nat Commun* 5:5103.
9. Vereecke L, et al. (2010) Enterocyte-specific A20 deficiency sensitizes to tumor necrosis factor-induced toxicity and experimental colitis. *J Exp Med* 207:1513–1523.

10. Afonina IS, Zhong Z, Karin M, Beyaert R (2017) Limiting inflammation-the negative regulation of NF-κB and the NLRP3 inflammasome. *Nat Immunol* 18:861–869.
11. Murphy SF, et al. (2014) Intestinal epithelial expression of TNFAIP3 results in microbial invasion of the inner mucus layer and induces colitis in IL-10-deficient mice. *Am J Physiol Gastrointest Liver Physiol* 307:G871–G882.
12. Rhee L, et al. (2012) Expression of TNFAIP3 in intestinal epithelial cells protects from DSS- but not TNBS-induced colitis. *Am J Physiol Gastrointest Liver Physiol* 303:G220–G227.
13. Wertz IE, et al. (2015) Phosphorylation and linear ubiquitin direct A20 inhibition of inflammation. *Nature* 528:370–375.
14. Wertz IE, et al. (2004) De-ubiquitination and ubiquitin ligase domains of A20 downregulate NF-kappaB signalling. *Nature* 430:694–699.
15. Wang L, Du F, Wang X (2008) TNF-alpha induces two distinct caspase-8 activation pathways. *Cell* 133:693–703.
16. Lu TT, et al. (2013) Dimerization and ubiquitin mediated recruitment of A20, a complex deubiquitinating enzyme. *Immunity* 38:896–905.
17. De A, Dainichi T, Rathinam CV, Ghosh S (2014) The deubiquitinase activity of A20 is dispensable for NF-κB signaling. *EMBO Rep* 15:775–783.
18. Kolodziej LE, et al. (2011) TNFAIP3 maintains intestinal barrier function and supports epithelial cell tight junctions. *PLoS One* 6:e26352.
19. Sato T, et al. (2009) Single Lgr5 stem cells build crypt-villus structures in vitro without a mesenchymal niche. *Nature* 459:262–265.
20. Vereecke L, Beyaert R, van Loo G (2009) The ubiquitin-editing enzyme A20 (TNFAIP3) is a central regulator of immunopathology. *Trends Immunol* 30:383–391.
21. Wallach D, Kang T-B, Dillon CP, Green DR (2016) Programmed necrosis in inflammation: Toward identification of the effector molecules. *Science* 352:aaf2154.
22. Degterev A, et al. (2008) Identification of RIP1 kinase as a specific cellular target of necrostatins. *Nat Chem Biol* 4:313–321.
23. Berger SB, et al. (2015) Characterization of GSK'963: A structurally distinct, potent and selective inhibitor of RIP1 kinase. *Cell Death Discov* 1:15009.
24. Mandal P, et al. (2014) RIP3 induces apoptosis independent of pronecrotic kinase activity. *Mol Cell* 56:481–495.
25. Polykratis A, et al. (2014) Cutting edge: RIPK1 kinase inactive mice are viable and protected from TNF-induced necroptosis in vivo. *J Immunol* 193:1539–1543.
26. Vanden Berghe T, Linkermann A, Jouan-Lanhouet S, Walczak H, Vandenabeele P (2014) Regulated necrosis: The expanding network of non-apoptotic cell death pathways. *Nat Rev Mol Cell Biol* 15:135–147.
27. Jaco I, et al. (2017) MK2 phosphorylates RIPK1 to prevent TNF-induced cell death. *Mol Cell* 66:698–710.e5.
28. Tenev T, et al. (2011) The ripoptosome, a signaling platform that assembles in response to genotoxic stress and loss of IAPs. *Mol Cell* 43:432–448.
29. Catrysse L, et al. (2016) A20 prevents chronic liver inflammation and cancer by protecting hepatocytes from death. *Cell Death Dis* 7:e2250.
30. Boone DL, et al. (2004) The ubiquitin-modifying enzyme A20 is required for termination of Toll-like receptor responses. *Nat Immunol* 5:1052–1060.
31. Kattah MG, et al. (2018) A20 and ABIN-1 synergistically preserve intestinal epithelial cell survival. *J Exp Med* 215:1839–1852.
32. Tokunaga F, et al. (2012) Specific recognition of linear polyubiquitin by A20 zinc finger 7 is involved in NF-κB regulation. *EMBO J* 31:3856–3870.
33. de Almagro MC, Goncharov T, Newton K, Vucic D (2015) Cellular IAP proteins and LUBAC differentially regulate necrosome-associated RIP1 ubiquitination. *Cell Death Dis* 6:e1800.
34. Lafont E, et al. (2017) The linear ubiquitin chain assembly complex regulates TRAIL-induced gene activation and cell death. *EMBO J* 36:1147–1166.
35. de Almagro MC, et al. (2017) Coordinated ubiquitination and phosphorylation of RIP1 regulates necroptotic cell death. *Cell Death Differ* 24:26–37.
36. Draber P, et al. (2015) LUBAC-recruited CYLD and A20 regulate gene activation and cell death by exerting opposing effects on linear ubiquitin in signaling complexes. *Cell Rep* 13:2258–2272.
37. Verhelst K, et al. (2012) A20 inhibits LUBAC-mediated NF-κB activation by binding linear polyubiquitin chains via its zinc finger 7. *EMBO J* 31:3845–3855.
38. Donepudi M, Mac Sweeney A, Briand C, Grütter MG (2003) Insights into the regulatory mechanism for caspase-8 activation. *Mol Cell* 11:543–549.
39. Pop C, Fitzgerald P, Green DR, Salvesen GS (2007) Role of proteolysis in caspase-8 activation and stabilization. *Biochemistry* 46:4398–4407.
40. Jin Z, et al. (2009) Cullin3-based polyubiquitination and p62-dependent aggregation of caspase-8 mediate extrinsic apoptosis signaling. *Cell* 137:721–735.
41. Onizawa M, et al. (2015) The ubiquitin-modifying enzyme A20 restricts ubiquitination of the kinase RIPK3 and protects cells from necroptosis. *Nat Immunol* 16:618–627.
42. Newton K, et al. (2014) Activity of protein kinase RIPK3 determines whether cells die by necroptosis or apoptosis. *Science* 343:1357–1360.
43. Dobin A, et al. (2013) STAR: Ultrafast universal RNA-seq aligner. *Bioinformatics* 29: 15–21.
44. Li B, Dewey CN (2011) RSEM: Accurate transcript quantification from RNA-seq data with or without a reference genome. *BMC Bioinformatics* 12:323.
45. Anders S, Huber W (2010) Differential expression analysis for sequence count data. *Genome Biol* 11:R106.
46. Meerbrey KL, et al. (2011) The pINDUCER lentiviral toolkit for inducible RNA interference in vitro and in vivo. *Proc Natl Acad Sci USA* 108:3665–3670.
47. Koo B-K, et al. (2011) Controlled gene expression in primary Lgr5 organoid cultures. *Nat Methods* 9:81–83.